Laser-Assisted Scalable Pore Fabrication in Graphene Membranes for Blue-Energy Generation

Sharad Kumar Yadav,[a, b, c] Manikandan D,[b] Chob Singh,[b] Mukesh Kumar,[b] Aswathy G,[b] Sundara Ramaprabhu,[b, d] Vishal V. R. Nandigana,[a] and Pramoda K. Nayak*[b, c, e, f]

The osmotic energy from a salinity gradient (i.e. blue energy) is identified as a promising non-intermittent renewable energy source for a sustainable technology. However, this membrane-based technology is facing major limitations for large-scale viability, primarily due to the poor membrane performance. An atomically thin 2D nanoporous material with high surface charge density resolves the bottleneck and leads to a new class of membrane material the salinity gradient energy. Although 2D nanoporous membranes show extremely high performance in terms of energy generation through the single pore, the fabrication and technical challenges such as ion concentration polarization make the nanoporous membrane a non-viable solution. On the other hand, the mesoporous and micro porous structures in the 2D membrane result in improved energy generation with very low fabrication complexity. In the present work, we report femtosecond (fs) laser-assisted scalable fabrication of μm to mm size pores on Graphene membrane for blue energy generation for the first time. A remarkable osmotic power in the order of μW has been achieved using mm size pores, which is about six orders of magnitudes higher compared to nanoporous membranes, which is mainly due to the diffusion-osmosis driven large ionic flux. Our work paves the way towards fs laser-assisted scalable pore creation in the 2D membrane for large-scale osmotic power generation.

Introduction

The world's heavy reliance on fossil fuels causing climate change at an unprecedented rate and there is the need of the hours to explore environment-friendly alternate energy sources to meet the growing energy demands.[1] In past decades, the salinity gradient energy (SGE), i.e. blue energy has gained more attention over solar and wind energy because of no intermittency issue.[2] The pressure retarded osmosis (PRO) and reverse electrodialysis (RED) are the two most focused membrane-based technology in harnessing blue energy.[3–7] The PRO is based on water selective transport[8] whereas the RED relies on ion-selective transport.[9–15] A wide range of membrane materials has been demonstrated so far for SGE, including polymeric membranes,[11–13] solid-state metal oxides membranes,[6,7] hybrid composite membranes,[13,14,19–21] and metal-organic composite membranes.[15] Recently, the low-dimensional materials such as Graphene,[14,15] and MoS_2[16–18] show high energy extraction efficiencies that are several orders of magnitude higher compared to the conventional membranes because of the ion transport through these membrane scales with membrane thickness and surface charge density. These materials are gaining the lead in RED technology as they offer high selectivity and remarkably high conductance.[16–21] The experimentally demonstrated power using the intrinsic defect in graphene is 10 pW (with a single nanopore) and the estimated power density is 700 Wm^{-2}.[14,15] With the single nano-pore in nanoconfined boron nitride (BNNT), the reported power is 20 pW and the estimated power density is 4 kWm^{-2}.[29] More recently, all-time high conductance has been reported in single nano-pore MoS_2, showing 1.2 to 2.8 pW power with an estimated power density of 1 MWm^{-2}.[25]

The use of nanoporous membranes creates a huge impact in SGE, where the ion transport under nanoscale confinement plays a crucial role to understand the viable energy technology.[22–29] However, the ionic current inside nanoporous membranes cannot be predicted accurately using the pore dimensions,[24] and the surface charge density influences the ion transport resulting in surface-charge governed transport.[30–32] Moreover, it has been predicted that multiple nanopores have advantages over single nanopores in terms of current density.[41] There are many techniques available to create the nanopores including transmission electron microscope (TEM) drilling,[42]

[a]   S. K. Yadav, V. V. R. Nandigana
      Department of Mechanical Engineering,
      Indian Institute of Technology Madras,
      Chennai 600036, India
[b]   S. K. Yadav, M. D, C. Singh, M. Kumar, A. G, S. Ramaprabhu, P. K. Nayak
      Department of Physics,
      Indian Institute of Technology Madras,
      Chennai 600 036, India
      E-mail: pnayak@iitm.ac.in
[c]   S. K. Yadav, P. K. Nayak
      Micro Nano and Bio-Fluidics Group,
      Indian Institute of Technology Madras,
      Chennai-600036, India
[d]   S. Ramaprabhu
      Alternative Energy and Nanotechnology Laboratory (AENL),
      Nano Functional Materials Technology Centre (NFMTC),
      Indian Institute of Technology Madras,
      Chennai, India
[e]   P. K. Nayak
      2D Materials Research and Innovation Group,
      Indian Institute of Technology Madras,
      Chennai-600036, India
[f]   P. K. Nayak
      Centre for Nano and Material Sciences,
      Jain (Deemed-to-be University),
      Jain Global Campus, Kanakapura, Bangalore 562112, India

electrochemical reaction (ECR),[30,31] focused ion beam (FIB),[35,36] and so on. These techniques have their pros and cons and the controlled synthesis of multiple nanopores using these techniques is incredibly challenging. Hence, the osmotic power generation using 2D nanoporous membranes has become non-viable[45] due to the fabrication and technical challenges including large-area growth of 2D membrane, clean room requirement, lithography steps, and complex and slow pore drilling process. Such a tiny nm size pore in the membrane also limits the ionic flux during the transport, thereby hindering the ionic current or conductance per pore.[46] In addition, the single nanopore performance extrapolation to multiple nanopores is severely hampered by ionic concentration polarization (ICP)[45] The other challenging aspect is the requirement of a highly treated/filtered solution for the nanoporous membrane to avoid nanopore blockage. However, in the case of larger pore size (μm to mm) minimal or no water filtration is required.

In recent years, femtosecond (fs) laser micromachining has been considered as an effective alternate micromachining system over conventional photochemical[47] and reactive ion etching processes.[48] The conventional micromachining process involves a low processing rate, availability of micro-mask in etching area,[41,42] and a complex processing step,[51] whereas the fs laser micro-machining has the advantages such as a non-contact process, faster etching rate, multiple pores (MP) in fabrication in a single step, and non-masking process.[52]

In the present work, we have fabricated fs laser-assisted scalable μm and mm size pores on a 2D Graphene/Copper (Gr/Cu) membrane for blue energy generation. The μm and mm size pores have advantages over nanopores in terms of current density and avoid the technical challenges of fabricating multiple nanopores. The osmotic power was measured using a pair of Pt electrodes placed across two salt solutions of different concentrations separated by Gr/Cu membrane in a typical diffusion cell experiment. We have achieved an osmotic power in the order of μW using μm and mm size pores, which is about six orders of magnitudes higher compared to nanoporous membranes. Our work paves the way towards fs laser-assisted scalable pore creation in the 2D membrane for large-scale osmotic power generation.

Experimental Methods

Fabrication of Micrometer-to-Millimeter-Sized Pores in 2D Gr/Cu Membranes Using Femtosecond Laser-based Micromachining

Commercially available Gr/Cu (18 μm) membranes with dimensions (10 mm×10 mm) were procured from Graphenea USA. The basic characterizations of Gr/Cu membrane including Raman, scanning electron micrographs (SEM) and optical micrographs (OM) are shown in supporting information (Figures S1 and S2). Pores with different dimensions such as 500 μm, 1 mm, and 2 mm with single and multiple (four) pores were fabricated in this Gr/Cu sheet using the fs laser. Different types of drilling methods were employed depending upon the pore radius. Percussion drilling, in which the laser pulse shaped to a particular sized voxel is focused on the desired location for a required time to ablate the material with a

geometric size that is identical to the size of the voxel. Using this technique, the pores of dimensions 500 μm, 1 mm and 2 mm were created. Moreover, multiple numbers of pores were also fabricated in this membrane since the power generation can be increased by increasing the pore density. The schematic of the fs laser micro-machining setup and the associated parameters are shown in Figure 1.

Blue-Energy-Generation Setup

Creating a concentration gradient in mm-sized pores is a challenge, where often mixing of solutions will happen immediately. However, this challenge can be overcome by maintaining the constant concentration gradient across the membrane by continuously supplying the new solution of the same concentration and optimizing the diffusion cell design such that the mixed solution should be taken out simultaneously. For this purpose, we have designed, calibrated, and validated an automated experimental setup for the ion transport measurements in our recent work.[53] This set up was used to measure SGE using this porous Gr/Cu membrane, which we named as blue energy generator as shown in Figure S3.

Results and Discussion

I–V Characteristics of Micrometer-to-Millimeter-Sized Pore Gr/Cu Membranes Using a Salinity Gradient

The I–V characteristics of Gr/Cu membranes with SP and MP were measured with three salinity gradient concentrations $\nabla C = 40$, $\nabla C = 100$, and $\nabla C = 1000$. The KCl solution was used in the experiment, as the K^+ and Cl^- ions have nearly the same hydration size and mobility.[45,46] The three KCl concentrations 0.5 M, 0.6 M, 6 mM, 13 mM and 0.6 mM are used to create salinity gradient $\nabla C = 40$, $\nabla C = 100$, and $\nabla C = 1000$. Figure 2 shows the short-circuit current and open-circuit voltage for the SP and MP of size 500 μm, 1 mm, and 2 mm at $\nabla C = 40$, $\nabla C = 100$, and $\nabla C = 1000$. The short-circuit current value is found to be in the order of μW and it increases with an increase in pore size as well as the number of pores. The osmotic power has been calculated from the I–V curves
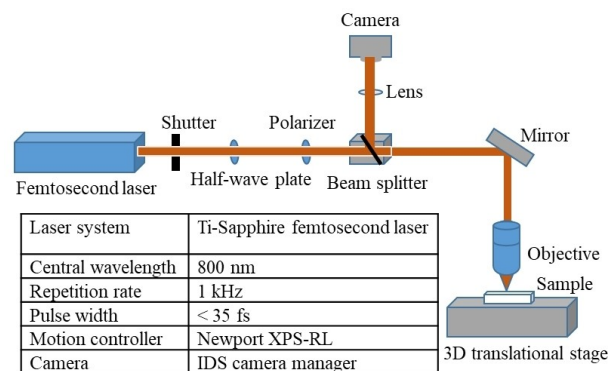

Laser system	Ti-Sapphire femtosecond laser
Central wavelength	800 nm
Repetition rate	1 kHz
Pulse width	< 35 fs
Motion controller	Newport XPS-RL
Camera	IDS camera manager

Figure 1. Schematic set up of fs laser micromachining set up and the associated parameters used to fabricate 500 μm, 1 mm, and 2 mm pore on Gr/Cu membrane of dimension 10 mm ×10 mm.
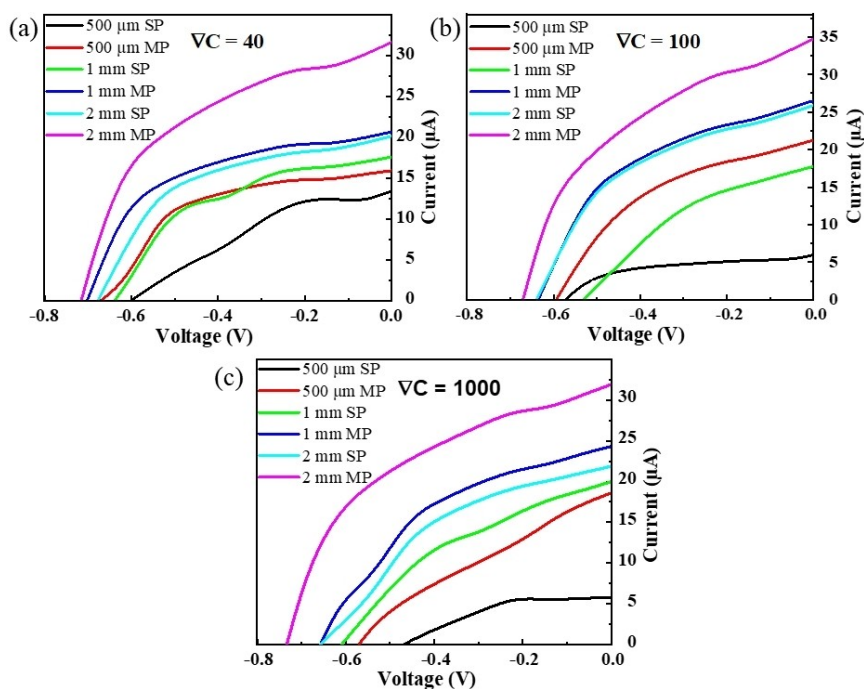
ChemPhysChem

Research Article
doi.org/10.1002/cphc.202200598

**Chemistry
Europe**

European Chemical
Societies Publishing

Figure 2. The I–V characteristic plot **(a)** with $\nabla C = 40$, **(b)** with $\nabla C = 100$, and **(c)** with $\nabla C = 1000$, for different pore dimensions.

(Figure 3) and the values are mentioned in Table 1. It is observed that the magnitude of the power increases with the increase in pore size and this is because larger pores allow the higher ion flux through it,[46] thereby generating higher power compared to nanopores which limit the ion flux (Table 2). With the increase in the number of pores for the same dimension, although the power increases, it does not scale accordingly as the performance of multiple pores cannot be extrapolated
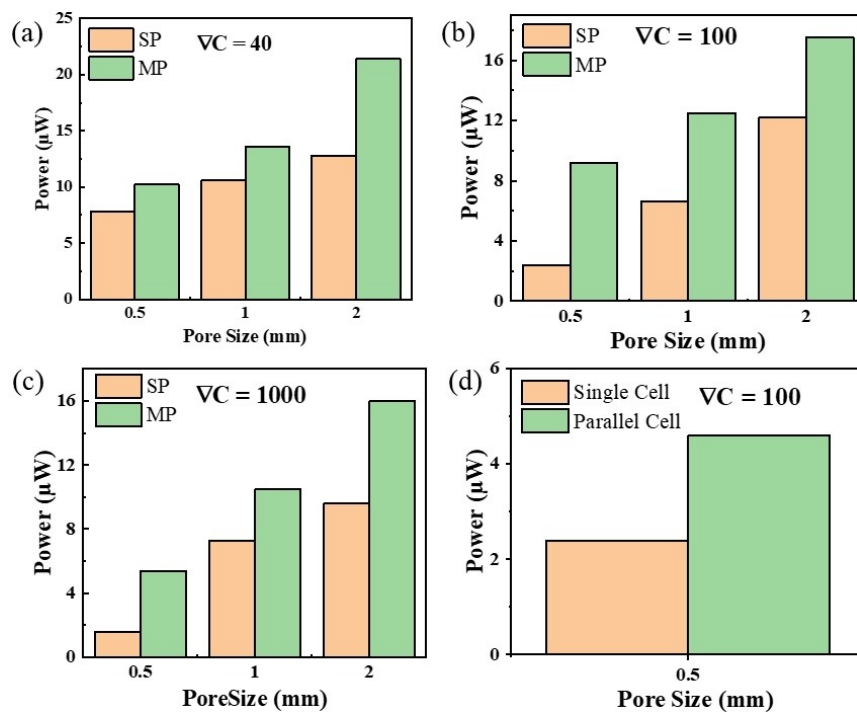

Figure 3. The power histogram plot **(a)** with $\nabla C = 40$, **(b)** with $\nabla C = 100$, and **(c)** with $\nabla C = 1000$, and **(d)** with with $\nabla C = 100$ in single cell and parallel configuration for different pore dimensions.

ChemPhysChem

Research Article
doi.org/10.1002/cphc.202200598

Chemistry Europe
European Chemical
Societies Publishing

Table 1. The performance of different materials and pore dimensions used for osmotic energy generation.

Pore diameter	Number of pores	Power (P=$V_{oc} \times I_{sc}$)			Porosity
		$\triangle C = 40$	$\triangle C = 100$	$\triangle C = 1000$	
500 μm	Single	7.8 μW	2.4 μW	1.6 μW	0.7 %
500 μm	Four	10.2 μW	9.2 μW	5.4 μW	1.5 %
1 mm	Single	10.6 μW	6.6 μW	7.3 μW	2.7 %
1 mm	Four	13.6 μW	12.5 μW	10.5 μW	6.2 %
2 mm	Single	12.8 μW	12.2 μW	9.6 μW	11.1 %
2 mm	Four	21.4 μW	17.5 μW	16 μW	25 %

Table 2. The performance of different membrane materials and pore dimensions used for osmotic power generation.

Material Used	Pore Dimension	Power (P=$V_{oc} \times I_{sc}$)	Refs.
hBN/SiN	6 nm pore, 3X3 pore array, 12 nm length.	2.3 nW	[41]
PET.	405 nm canonical pore, 12 μm length	3.2 nW	[46]
MoS$_2$.	2-20 nm pore, 0.65 nm length	1 nW	[25]
Graphene	0.4-10 nm pore, 0.34 nm length	10 pW	[22]
hBN nanotube	15-40 nm pore, 1 μm length	20 pW	[29]
Gr/Cu	500 μm pore, 18 μm length	7.8 μW	Present Work

based on single pore performance. The generated osmotic power in the present work shows three to six order improvement in compared to different membranes of various pore size reported by other research groups so far (see Table 2). It can be noted that we are calculating and comparing the power per pore similar to earlier report,[24] but not the power density (since the selectivity is purely absent in this case which is shown latter in numerical simulation section).

The magnitudes of open-circuit voltage, short-circuit current and eventually the generated power at $\nabla C = 40$ are higher compared to $\nabla C = 100$ and $\nabla C = 1000$. While preparing the concentration gradient for $\nabla C = 40$, the higher concentration side was 0.5 mol KCl and the lower concentration side was 13 mmol KCl. In the case of $\nabla C = 100$, these concentrations were 0.6 mol KCl and 6 mmol KCl, and for $\nabla C = 1000$, these values were 0.6 mol KCl and 0.6 mmol KCl. The lower concentrated KCl solution offers higher resistance than the higher concentrated KCl solution.[56] Hence, the short-circuit current and the osmotic power values were lower in the case of $\nabla C = 100$ compared to $\nabla C = 100$ and $\nabla C = 40$ as shown in Figure 3.

It can be noted that the conducting material (Gr/Cu) is taken as the membrane in the present work, where the electronic conduction current is also contributing to the power generation in addition to ionic current. Even when the Gr/Cu membrane does not have any pore into it, a finite conduction current (*i.e.*, short-circuit) and the voltage (*i.e.*, open-circuit) are recorded (Figure 4). The electrochemical potential of different concentration solutions causes the potential difference which is acting as an electromotive force for the conduction current.[57] Due to the presence of pores in the membrane, the current value rises as the ionic current superimposes (modulates) the conduction current (Figure 2). In order to get rid of the
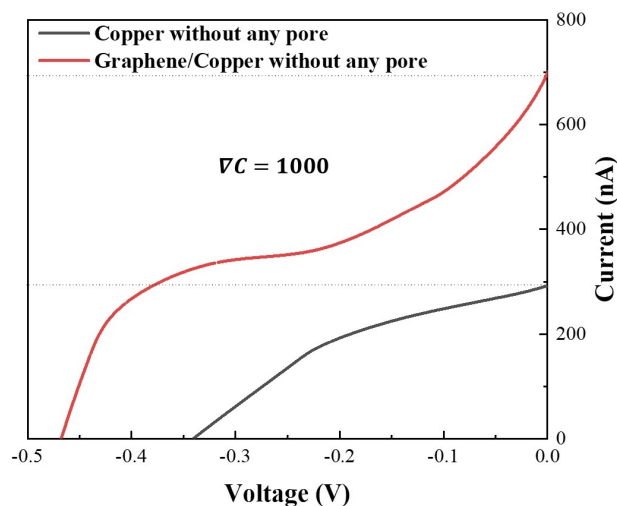

Figure 4. The I–V characteristic plot without any pore using copper and Gr/Cu membrane.

electronic conduction effect, we have also carried out the transport measurement using a pure insulating silicone membrane (with 1 mm diameter single pore) shown in Figure S8. With the silicone membrane, the maximum power observed is 45.1 nW. However, the maximum power due to Cu and Gr/Cu membrane without any pore is 98.3 nW and 327.6 nW, respectively (which is due electronic contribution, not the ionic). The maximum power with 1 mm diameter single pore using Gr/Cu membrane is 6.6 μW (Figure 3), which is three orders of magnitude higher than insulating silicone membrane of same pore dimension. This indicates that the power generation in larger size pore Gr/Cu membrane is mostly due to ion transport.

Effect of Graphene and Membrane Size on Osmotic Power

We have also analyzed the effect of graphene and membrane size on osmotic power generation. Beginning with the graphene effect, the 500 μm SP in Gr/Cu membrane shows higher power compared to the identical copper membrane without graphene (Figure S5). The higher conductivity and negative surface charge density of graphene offer higher current and the higher voltage across the membrane respectively.[2,49] On the other hand, the membrane size does not affect the osmotic power performance as it is shown in (Figure S6). The larger area membrane (1 inch × 1 inch) is used to analyze the effect of membrane size on generated osmotic power. With the 500 μm SP and 1 mm SP, the generated osmotic power using 10 mm × 10 mm membrane is 2.4 μW and 6.6 μW respectively, whereas for the same pore sizes, the generated osmotic power using 1 inch × 1 inch membrane is 2.2 μW and 7.2 μW, respectively.

As the ion flux is in a perpendicular direction to the membrane, so the membrane size does not play any role in the osmotic performance. To maximize the power generation, we have considered two 500 μm SP in a parallel configuration and observed that the generated power is nearly doubled in comparison to a SP (See Figure 3d). Hence from the above observation, it is clear that cascading of pores has advantages in generating higher osmotic power compared to SP alone. Furthermore, in comparison to nanopores, the micro and mm size pores show better power performance despite compromise with the ion selectivity (Table 2).

The origin of the power generation in larger size pore is may be due to the diffusion osmosis driven large ionic flux. The diffusio-osmosis mechanism is driven by the osmotic pressure gradient in the vicinity of the surface of the porous membrane.[2,29] It does not require the semipermeable membrane for the osmotic flow because it results from specific interactions between the solute (in this case, a salt) and the surface (Gr/Cu).[2] The concentration gradient along the surface of the porous membrane causes an electric current (ion-driven current), known as the diffusio-osmotic current (I_{osm}), as the ions move under the interfacial osmotic pressure gradient.[2,29,59,60] Our experimental setup is designed to maintain the concentration gradient across the membrane, as reported earlier.[53] Hence, the diffusion-osmosis current can be harvested using the larger pore by maintaining the specific concentration gradient across the membrane.

Effect of Ion Selectivity

The observation of higher power generation in the mm-size pores in comparison to nanopores is attributed to the diffuso-osmosis driven ion transport. It is well known that ion selectivity plays an important role in power generation at the nanoscale. To understand the influence of the ion selectivity of the membrane on ion transport characteristics in our experiments,

we carried out the COMSOL simulations. The origin of the ion selectivity is mainly due to the electrical double-layer thickness and the surface potential (in the case of conducting surfaces)/ surface charge (in the case of non-conducting surfaces). In general, the discrete size effects of ions and ion-water interactions[69,70] are disregarded in these simulations as they do not play an important role in determining the ion selectivity of the pores at the nanoscale.[25,71–75] So, we adapted the continuum scale models to study the ion selectivity effects and the formulations based on the Poisson-Nernst-Plank (PNP), and Navier-Stokes (NS) equations were developed.[61–68] The distribution of ionic concentration (c), potential (ϕ), and velocity (U) is calculated by numerically solving these equations (1–4) in a coupled way in the stationary condition using COMSOL Multiphysics and are given below,

$$\frac{\partial c_i}{\partial t} = -\nabla.J_i = -\nabla.\left(c_i\, U_i - D_i\, \nabla c_i - \frac{F\, z_i D_i c_i}{RT}\nabla\varphi \right) \qquad (1)$$

$$\nabla.(\varepsilon_o \varepsilon_r \nabla\varphi) = -\rho_e \qquad (2)$$

$$\rho\left(\frac{\partial U}{\partial t} + U.\,\nabla U \right) = -\nabla p + \mu\nabla^2 U - \rho_e\nabla\varphi \qquad (3)$$

$$\nabla U = 0 \qquad (4)$$

Where J – total flux of the ionic species, $i = 1, 2$ – no of species, z – valency, D – diffusion coefficient of ions, F – Faraday constant, R – universal gas constant, T – temperature, $\varepsilon_o, \varepsilon_r$ – relative permittivity of medium and free space, ρ – density of the fluid, μ – viscosity, p – pressure and ρ_e – space charge density ($\rho_e = F\sum z_i c_i$).

The following boundary conditions were considered in this work.

(i) The constant surface potential (φ_s) is considered at all pore surfaces to represent the conducting surface in our simulations, and all pore surfaces are considered to be impermeable to the ions with no slip.

(ii) Top reservoir walls are considered to slip ($n.\, U = 0$) and are impermeable to the ions.

(iii) Higher concentration (C_H) and lower concentration (C_L) are assumed at the ends of the left and right reservoirs, respectively.

(iv) Further, no external pressure and voltages are considered in our simulations.

Here, COMSOL simulations elucidate the variation of the ion selectivity of the pores over a wide range of diameters and the surface potential. Figure 5a shows the variation of the cation selectivity (t+) with the diameter of the pores. Here, the (t+) is calculated using the following relation,
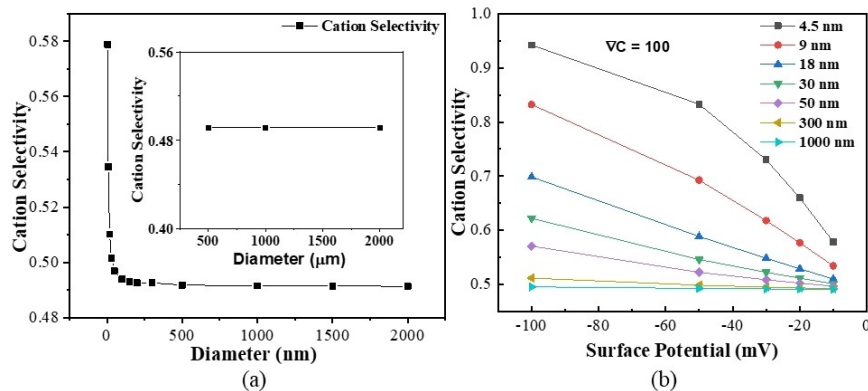
ChemPhysChem

Research Article
doi.org/10.1002/cphc.202200598

**Chemistry
Europe**
European Chemical
Societies Publishing

Figure 5. The variation of the cation selectivity with **(a)** the pore diameter and **(b)** the surface potential (φ_s) for the assumed concentration gradient (∇C) of 100 across the reservoirs. Here, the conducting pore surface is represented using constant surface potential ($\varphi_s = -10\ mV$).

$$t^+ = \frac{|I^+|}{|I^+| + |I^-|} \qquad (5)$$

Where, I^+, I^- represents the ionic current carried by the cations (K^+) and anions (Cl^-). It is noted that the (t^+) drastically reduces to the value of 0.5 as the pore diameter increases since the thickness of the electrical double layer (EDL) is negligible at this larger diameter. The ion selectivity depends on the thickness of the EDL and the surface potential/charge density.[9,76,77] Further, with the increase in the surface potential (φ_s), the cation selectivity increases for a smaller pore diameter, whereas it remains almost the same for a larger pore diameter (Figure 5b). Moreover, when the pore diameter exceeds 30 nm, it completely loses the ion selectivity, and the ion transport happens due to the bulk effect. Similarly, it can be extended to mm size pores as shown in inset of Figure 5(a).

Conclusions

In conclusion, the fs-laser-assisted scalable pore fabrication in Gr/Cu membrane for the giant blue energy generation was presented. The fabrication and technical advantage of micro and mm size pores over the nanopores were discussed. We have achieved an osmotic power in the order of μW using μm to mm size pores, which is about six orders of magnitudes higher compared to the nano pores. The origin of the enhanced osmotic power in the case of μm to mm size pores is due to diffusion-osmosis driven large ionic transport. The power generated using MP was higher than a SP of the same dimension. The membrane size did not affect the power performance. A parallel configuration of such a system with an optimized diffusion cell to pore diameter could provide larger power with a higher surface charge density. This present work paves the way towards fs laser-assisted scalable pore creation in the 2D membrane for large-scale osmotic power generation.

Conflict of Interest

The authors declare no conflict of interest.

Data Availability Statement

The data that support the findings of this study are available from the corresponding author upon reasonable request.

[1] IPCC Report, https://www.ipcc.ch/site/assets/uploads/2018/02/AR5_SYR_FINAL_SPM.pdf.
[2] A. Siria, M.-L. Bocquet, L. Bocquet, *Nat. Chem. Rev.* **2017**, *1*, 0091.
[3] S. Kang, J. Li, Z. Wang, C. Zhang, X. Kong, *J. Power Sources* **2022**, *519*, 230806.
[4] B. Muhthassim, X. K. Thian, K. N. Md Hasan, *IOP Conf. Ser. Earth Environ. Sci.* **2018**, *140*, 12045.
[5] Z. Jalili, K. W. Krakhella, K. E. Einarsrud, O. S. Burheim, *J. Energy Storage* **2019**, *24*, 100755.
[6] G. Z. Ramon, B. J. Feinberg, E. M. V Hoek, *Energy Environ. Sci.* **2011**, *4*, 4423.
[7] K. Nijmeijer, S. Metz, *Sustain. Sci. Eng.* **2010**, *2*, 95–139.
[8] K. Cao, Z. Jiang, X. Zhang, Y. Zhang, J. Zhao, R. Xing, S. Yang, C. Gao, F. Pan, *J. Membr. Sci.* **2015**, *490*, 72–83.

ChemPhysChem

Research Article
doi.org/10.1002/cphc.202200598

Chemistry
Europe
European Chemical
Societies Publishing

[9] G. Di Muccio, B. Morozzo della Rocca, M. Chinappi, *ACS Nano* **2022**, *16*, 8716–8728.

[10] A. Emdadi, J. Hestekin, L. F. Greenlee, *Sustain. Energy Fuels* **2021**, *5*, 6135–6144.

[11] S. H. Kwak, S. R. Kwon, S. Baek, S. M. Lim, Y. C. Joo, T. D. Chung, *Sci. Rep.* **2016**, *6*, 26416.

[12] S. W. Lee, H. J. Kim, D. K. Kim, *Energies* **2016**, *9*, 49.

[13] W. Xin, Z. Zhang, X. Huang, Y. Hu, T. Zhou, C. Zhu, X.-Y. Kong, L. Jiang, L. Wen, *Nat. Commun.* **2019**, *10*, 3876.

[14] Z. Zhang, L. He, C. Zhu, Y. Qian, L. Wen, L. Jiang, *Nat. Commun.* **2020**, *11*, 875.

[15] R. Li, J. Jiang, Q. Liu, Z. Xie, J. Zhai, *Nano Energy* **2018**, *53*, 643–649.

[16] X. Liu, M. He, D. Calvani, H. Qi, K. B. S. S. Gupta, H. J. M. de Groot, G. J. A. Sevink, F. Buda, U. Kaiser, G. F. Schneider, *Nat. Nanotechnol.* **2020**, *15*, 307–312.

[17] C. Y. Lin, C. Combs, Y. S. Su, L. H. Yeh, Z. S. Siwy, *J. Am. Chem. Soc.* **2019**, *141*, 3691.

[18] S. Balme, T. Ma, E. Balanzat, J. M. Janot, *J. Membr. Sci.* **2017**, *544*, 18–24.

[19] C. Zhang, T. Xiao, B. Lu, J. He, Y. Wang, J. Zhai, *Small* **2022**, *18*, 2270104.

[20] S. Hou, Q. Zhang, Z. Zhang, X. Kong, B. Lu, L. Wen, L. Jiang, *Nano Energy* **2021**, *79*, 105509.

[21] Q.-Y. Wu, C. Wang, R. Wang, C. Chen, J. Gao, J. Dai, D. Liu, Z. Lin, L. Hu, *Adv. Energy Mater.* **2020**, *10*, 1902590.

[22] R. C. Rollings, A. T. Kuan, J. A. Golovchenko, *Nat. Commun.* **2016**, *7*, 11408.

[23] M. I. Walker, K. Ubych, V. Saraswat, E. A. Chalklen, P. Braeuninger-Weimer, S. Caneva, R. S. Weatherup, S. Hofmann, U. F. Keyser, *ACS Nano* **2017**, *11*, 1340–1346.

[24] M. Macha, S. Marion, V. V. R. Nandigana, A. Radenovic, *Nat. Rev. Mater.* **2019**, *4*, 588–605.

[25] J. Feng, M. Graf, K. Liu, D. Ovchinnikov, D. Dumcenco, M. Heiranian, V. Nandigana, N. R. Aluru, A. Kis, A. Radenovic, *Nature* **2016**, *536*, 197–200.

[26] J. Feng, K. Liu, M. Graf, M. Lihter, R. D. Bulushev, D. Dumcenco, D. T. L. Alexander, D. Krasnozhon, T. Vuletic, A. Kis, A. Radenovic, *Nano Lett.* **2015**, *15*, 3431–3438.

[27] H. Cheng, Y. Zhou, Y. Feng, W. Geng, Q. Liu, W. Guo, L. Jiang, *Adv. Mater.* **2017**, *29*, 1700177.

[28] S. Hong, F. Ming, Y. Shi, R. Li, I. S. Kim, C. Y. Tang, H. N. Alshareef, P. Wang, *ACS Nano* **2019**, *13*, 8917–8925.

[29] A. Siria, P. Poncharal, A.-L. Biance, R. Fulcrand, X. Blase, S. T. Purcell, L. Bocquet, *Nature* **2013**, *494*, 455–458.

[30] R. E. PATTLE, *Nature* **1954**, *174*, 660.

[31] R. S. Norman, *Science (80).* **1974**, *186*, 350–352.

[32] K. Tomabechi, *Energies* **2010**, *3*, 686–695.

[33] A. Dai, K. E. Trenberth, *J. Hydrometeorol.* **2002**, *3*, 660–687.

[34] F. Helfer, C. Lemckert, Y. G. Anissimov, *J. Membr. Sci.* **2014**, *453*, 337–358.

[35] N. Y. Yip, M. Elimelech, *Environ. Sci. Technol.* **2012**, *46*, 5230–5239.

[36] S. Sarp, Z. Li, J. Saththasivam, *Desalination* **2016**, *389*, 2–14.

[37] O. Schaetzle, C. J. N. Buisman, *Engineering* **2015**, *1*, 164–166.

[38] Q. Xie, F. Xin, H. G. Park, H. Duan, *Nanoscale* **2016**, *8*, 19527–19535.

[39] H. Daiguji, P. Yang, A. Majumdar, *Nano Lett.* **2004**, *4*, 137–142.

[40] D. Stein, M. Kruithof, C. Dekker, *Phys. Rev. Lett.* **2004**, *93*, 035901.

[41] K. Yazda, K. Bleau, Y. Zhang, X. Capaldi, T. St-Denis, P. Grutter, W. W. Reisner, *Nano Lett.* **2021**, *21*, 4152–4159.

[42] M. Graf, M. Lihter, M. Thakur, V. Georgiou, J. Topolancik, B. R. Ilic, K. Liu, J. Feng, Y. Astier, A. Radenovic, *Nat. Protoc.* **2019**, *14*, 1130–1168.

[43] P. Fürjes, Z. Fekete, L. Illés, A. L. Tóth, G. Battistig, R. E. Gyurcsányi, *Procedia Eng.* **2012**, *47*, 684–687.

[44] Y. H. Lanyon, G. De Marzi, Y. E. Watson, A. J. Quinn, J. P. Gleeson, G. Redmond, D. W. M. Arrigan, *Anal. Chem.* **2007**, *79*, 3048–3055.

[45] L. Wang, Z. Wang, S. K. Patel, S. Lin, M. Elimelech, *ACS Nano* **2021**, *15*, 4093–4107.

[46] M. Gao, P.-C. Tsai, Y.-S. Su, P.-H. Peng, L.-H. Yeh, *Small* **2020**, *16*, 2006013.

[47] L. Jiang, R. Cheung, M. Hassan, A. J. Harris, J. S. Burdess, C. A. Zorman, M. Mehregany, *J. Vac. Sci. Technol. B Microelectron. Nanom. Struct.* **2003**, *21*, 2998.

[48] A. Szczesny, P. Śniecikowski, J. Szmidt, A. Werbowy, *Vacuum* **2003**, *70*, 249–254.

[49] M. Farsari, G. Filippidis, S. Zoppel, G. A. Reider, C. Fotakis, *J. Micromech. Microeng.* **2005**, *15*, 1786–1789.

[50] C. Li, X. Shi, J. Si, T. Chen, F. Chen, S. Liang, Z. Wu, X. Hou, *Opt. Commun.* **2009**, *282*, 78–80.

[51] V. Khuat, Y. Ma, J. Si, T. Chen, F. Chen, X. Hou, *Appl. Surf. Sci.* **2014**, *289*, 529–532.

[52] A. N. Samant, N. B. Dahotre, *J. Eur. Ceram. Soc.* **2009**, *29*, 969–993.

[53] S. K. Yadav, M. Kumar, S. Ramaprabhu, V. V. R. Nandigana, P. K. Nayak, *Rev. Sci. Instrum.* **2022**, *93*, 64104.

[54] R. W. Impey, P. A. Madden, I. R. McDonald, *J. Phys. Chem.* **1983**, *87*, 5071–5083.

[55] J. N. Israelachvili, in *Intermolecular and Surface Forces, ed. J. N. B. T. I., S. F. (Third E. Israelachvili, Elsevier, San Diego* **2011**, pp. 71–90.

[56] M. Fromm, S. G. Schultz, *J. Membr. Biol.* **1981**, *62*, 239–244.

[57] S. W. Boettcher, S. Z. Oener, M. C. Lonergan, Y. Surendranath, S. Ardo, C. Brozek, P. A. Kempler, *ACS Energy Lett.* **2021**, *6*, 261–266.

[58] J. Gao, Y. Feng, W. Guo, L. Jiang, *Chem. Soc. Rev.* **2017**, *46*, 5400–5424.

[59] J. L. Anderson, *Annu. Rev. Fluid Mech.* **1989**, *21*, 61–99.

[60] H. Maddah *ARPN Journal of Engineering and Applied Sciences* **2020**, *15*, 46–51.

[61] Y. Qiu, R. A. Lucas, Z. S. Siwy, *J. Phys. Chem. Lett.* **2017**, *8*, 3846–3852.

[62] C.-Y. Lin, P.-H. Wong, P.-H. Wang, Z. S. Siwy, L.-H. Yeh, *ACS Appl. Mater. Interfaces* **2020**, *12*, 3198–3204.

[63] L. Luo, D. A. Holden, W.-J. Lan, H. S. White, *ACS Nano* **2012**, *6*, 6507–6514.

[64] L. Luo, D. A. Holden, H. S. White, *ACS Nano* **2014**, *8*, 3023–3030.

[65] C.-Y. Lin, F. Chen, L.-H. Yeh, J.-P. Hsu, *Phys. Chem. Chem. Phys.* **2016**, *18*, 30160–30165.

[66] J. A. Wood, A. M. Benneker, R. G. H. Lammertink, *J. Phys. Condens. Matter* **2016**, *28*, 114002.

[67] A. M. Benneker, H. D. Wendt, R. G. H. Lammertink, J. A. Wood, *Phys. Chem. Chem. Phys.* **2017**, *19*, 28232–28238.

[68] I. I. Ryzhkov, A. V Minakov, *J. Membr. Sci.* **2016**, *520*, 515–528.

[69] C. Bakli, S. Chakraborty, *Nanoscale* **2019**, *11*, 11254–11261.

[70] C. Bakli, S. Chakraborty, *Nanoscale* **2016**, *8*, 6535–6541.

[71] T.-W. Lin, J.-P. Hsu, C.-Y. Lin, S. Tseng, *J. Phys. Chem. C* **2019**, *123*, 12437–12443.

[72] J.-Y. Lin, C.-Y. Lin, J.-P. Hsu, S. Tseng, *Anal. Chem.* **2016**, *88*, 1176–1187.

[73] I. Vlassiouk, S. Smirnov, Z. Siwy, *Nano Lett.* **2008**, *8*, 1978.

[74] L. X. Cao, Q. Wen, Y. P. Feng, D. Y. Ji, H. Li, N. Li, L. Jiang, W. Guo, *Adv. Funct. Mater.* **2018**, *28*, 1804189.

[75] L. Ma, X. An, F. Song, Y. Qiu, *J. Phys. Chem. Lett.* **2022**, *13*, 5669–5676.

[76] R. Long, M. Li, X. Chen, Z. Liu, W. Liu, *Int. J. Heat Mass Transfer* **2021**, *171*, 121126.

[77] P. Ma, J. Zheng, D. Zhao, W. Zhang, G. Lu, L. Lin, Z. Zhao, Z. Huang, L. Cao, *Mater. (Basel, Switzerland)* **2021**, *14*, 7012.
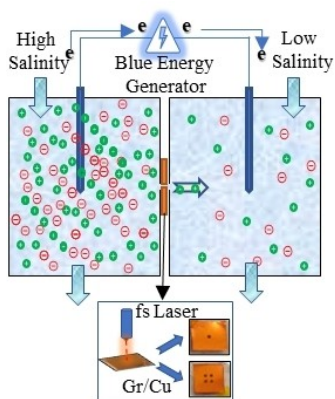
RESEARCH ARTICLE

Graphene-copper membranes with micro and millimeter pores show a higher osmotic power than nanopore membranes. Femtosecond lasers enable a faster, scalable, and simple pore fabrication process. Multiple-pore membranes show a higher power compared to the single-pore materials but are not able to extrapolate the single-pore performance.

S. K. Yadav, M. D, C. Singh, M. Kumar, A. G, S. Ramaprabhu, V. V. R. Nandigana, P. K. Nayak*

1 – 8

Laser-Assisted Scalable Pore Fabrication in Graphene Membranes for Blue-Energy Generation